Approximate Zero-Crossing: A new interpretable, highly discriminative and low-complexity feature for EEG and iEEG seizure detection

R Zanetti[1], U Pale[1], T Teijeiro[1,2] and D Atienza[1]

[1] Embedded Systems Laboratory(ESL), École Polytechnique Fédérale de Lausanne (EPFL), 1015, Lausanne, Switzerland
[2] Department of Mathematics, University of the Basque Country (UPV/EHU), Leioa, Spain

E-mail: `renato.zanetti@epfl.ch`

November 2022

Abstract.
   Objective: Long-term monitoring of people with epilepsy based on electroencephalography (EEG) and intracranial EEG (iEEG) has the potential to deliver key clinical information for personalised epilepsy treatment. More specifically, in outpatient settings, the available solutions are not satisfactory either due to poor classification performance or high complexity to be executed in resource-constrained devices (e.g., wearable systems). Therefore, we hypothesize that obtaining high discriminative features is the main avenue to improve low-complexity seizure-detection algorithms. *Approach*: inspired by how neurologists recognize ictal EEG data, and to tackle this problem by targeting resource-constrained wearable devices, we introduce a new interpretable and highly discriminative feature for EEG and iEEG, namely approximate zero-crossing (AZC). We obtain AZC by applying a polygonal approximation to mimic how our brain selects prominent patterns among noisy data and then using a zero-crossing count as a measure of the dominating frequency. By employing Kullback-Leiber divergence, leveraging CHB-MIT and SWEC-ETHZ iEEG datasets, we compare the AZC discriminative power against a set of 56 classical literature features (CLF). Moreover, we assess the performances of a low-complexity seizure detection method using only AZC features versus employing the CLF set. *Main results*: three AZC features obtained with different approximation thresholds are among the five with the highest median discriminative power. Moreover, seizure classification based on only AZC features outperforms an equivalent CLF-based method. The former detects 102 and 194 seizures, against 99 and 161 for the latter (CHB-MIT and SWEC-ETHZ, respectively). Moreover, the AZC-based method keeps a similar false-alarm rate (i.e., an average of 2.1 and 1.0, against 2.0 and 0.5, per day). *Significance*: we propose a new feature and demonstrate its capability in seizure classification for both scalp and intracranial EEG. We envision the use of such a feature to improve outpatient monitoring with resource-constrained devices.

1. Introduction

Epilepsy is a brain disease with a prevalence of 4–8 per 1000 population, placing it as the fourth most common neurological disorder worldwide [1]. Electroencephalography (EEG) is an essential tool for the diagnosis and management of people with epilepsy (PWE) [2]. According to electrode placement, EEG can be broadly divided into scalp and intracranial (iEEG) recordings. Scalp EEG acquisition is more affected by noise and artifacts but is non-invasive, thus more used in clinical practice [3]. When associated with video recordings, long-term EEG or iEEG monitoring can provide key clinical information for personalised epilepsy treatment (e.g., seizure count in a long period, monitoring for paroxysmal events, etc.) [4]. Such procedures are executed in-hospital, at epilepsy monitoring units (EMUs), over the course of several days, but normally once in the patient's lifetime due to the associated costs [5].

Conversely, outpatient assessment mainly relies on patient self-reports [6], which have been found to be prone to errors due to seizure unawareness, nocturnal events, and lack of patient commitment to keeping up with diaries [7]. Consequently, there is an unmet need for innovative solutions for automated outpatient monitoring [6, 8, 9]. However, commercially available products have been only certified for generalized tonic-clonic seizures (GTCS), which are associated with strong body movements, leaving most of the PWE unattended [10].

Several state-of-the-art (SoA) works have proposed methods for seizure detection based on EEG, potentially covering a greater number of seizure types [11, 13, 14, 15, 16, 3, 17, 18, 19, 12]. Yet, EEG-based outpatient monitoring is still a challenging problem as most of the proposed EEG-based methodologies are not feasible in the real world [9]. Besides the resource constraints for implementing some of the proposed solutions [13, 14], PWE also have demonstrated a strong preference for inconspicuous and non-stigmatizing monitoring devices [8, 6]. Hence, leveraging on their inherent unobtrusiveness, wearable devices offer considerable potential for supporting outpatient monitoring [10, 9]. However, a solution based on such devices entails the use of low-complexity algorithms due to the scarcity of resources (e.g., memory, processing, and battery capacity). Therefore, classical machine learning (ML) algorithms such as random forest (RF) and support vector machines (SVM) are fair candidates to comply with the above-described restrictions. First, these methods' models are relatively simple and fast to execute. In addition, they have been extensively used for EEG-/iEEG-based seizure detection [20]. Still, such algorithms should be optimized to achieve acceptable sensitivity and low false-alarm rates (FAR) [9].

Since ML algorithms tend to present marginal performance gains with the same input data and analysis conditions [21], we hypothesize that obtaining high discriminative features is an important avenue for improving low-complexity seizure-detection methods for resource-constrained wearable devices. In fact, when evaluating the EEG/iEEG signals acquired during long-term monitoring, neurologists are the ones setting the ground truth for ML algorithms. They are capable of identifying prominent ictal patterns among spontaneous EEG/iEEG, noise, and artifacts more accurately than SoA algorithms.

Thus, in this work, we introduce and evaluate a new feature of low-complexity for EEG and iEEG analysis, inspired by the way neurologists visually inspect signals, namely approximate zero crossing (AZC). To obtain the AZC, first, we simplify the EEG/iEEG signals by applying a polygonal approximation to mimic how our brain selects prominent patterns among noisy data. Then, we use a simple zero-crossing count as an estimation of the signal's dominating frequency. We assess the discriminative power of the AZC feature using the Kullback-Leiber (KL) divergence score [22]. Additionally, we design a low-complexity ML classification method based on RF and apply the time-series split cross-validation (TSCV) to assess the AZC feature performance in long-term seizure detection. As a comparison, we use the same method's recipe with a set of 56 classical literature features (CLF). Finally, we implement both strategies in a state-of-the-art wearable platform to assess its computational requirements. In all the previously mentioned tasks, we employ two publicly available datasets: the CHB-MIT Scalp (982.9 hours of data) [12] and the SWEC-ETHZ iEEG (2656 hours of data) [15]. The main contributions of this work are summarized in the following:

- A new interpretable feature of low-complexity towards resource-constrained wearable devices use, for automated seizure monitoring based on EEG and iEEG is presented. AZC shows a discriminative power higher than most of the other 56 features evaluated using the KL divergence in two widely used and publicly available long-term seizure monitoring datasets. Moreover, extracting the AZC features is 8.8x faster then calculating the CLF set of features.

- We propose the TSCV methodology for assessing the seizure classification performance, as we believe it presents results that are more realistic for a real-life long-term seizure monitoring application. To the best of our knowledge, it has not yet been used in EEG/iEEG-based seizure detection.

- We show that a ML solution of low-complexity based only on six AZC features achieves 100% sensitivity in 25 out of 42 subjects, plus nine
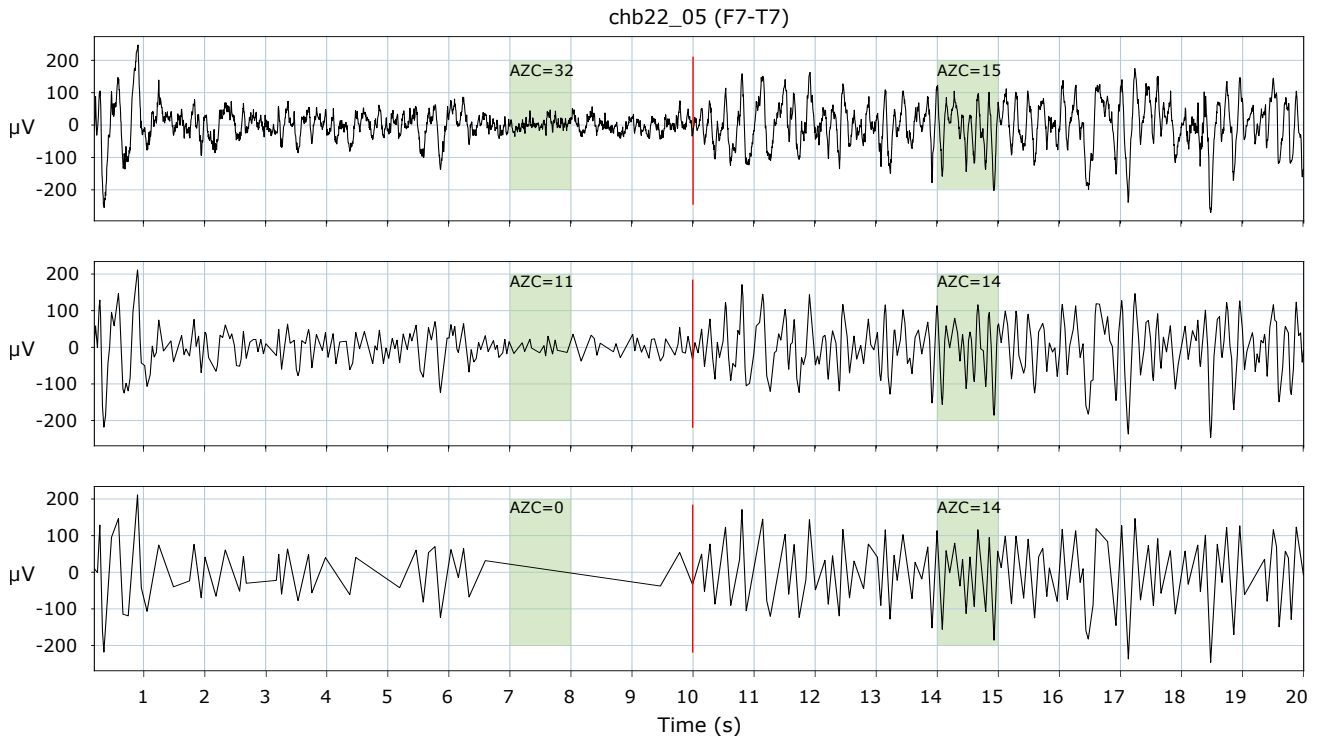
Figure 1. Illustrative example of the AZC feature, calculated at different approximation thresholds on a 20 *s* EEG window with a seizure starting at second 10. The top figure is the original signal, while the middle and the bottom ones are approximations with $\epsilon = 16$ and $\epsilon = 64$, respectively. [Source: Patient 22, file 25 from the CHB-MIT dataset.]

showing only one missing seizure. Moreover, the AZC-based method achieves a low FAR of 2.1 and 1.0/day on average for CHB-MIT and SWEC-ETHZ, respectively.

- We demostrated that the AZC-based classification method can outperform the CLF-based one for seizure detection: 102 and 194 seizures detected against 99 and 161 for CHB-MIT and SWEC-ETHZ, respectively.

The rest of the paper is organized as follows. Section 2 presents the AZC feature in detail and shows a visual example of how it works in real EEG data. In Section 3, we present our proposed methodology for assessing the discriminative power of the AZC feature and the training framework. Section 4 details the experimental setup for evaluating the proposed feature, whereas the results are presented in Section 5. We discuss these results in Section 6 and conclude this work in Section 7.

2. Approximate Zero-Crossing

We draw inspiration from clinical practice in EEG/iEEG screening for seizure patterns to develop the proposed AZC feature. AZC feature extraction method comprises two main steps. First, we simplify the signal using a polygonal approximation to mimic our brain's

capacity to find prominent patterns within noisy data. Second, we implement a zero-crossing count on the approximated signal. Therefore, in addition to a low computational complexity, the proposed AZC feature is easily interpretable. In the rest of this section, we detail our motivation, describe the algorithm to calculate the feature values, and show a visual example of how AZC varies with different thresholds for a real signal.

2.1. AZC: Motivation and Intuition

The basic objective of the AZC feature is to estimate the number of peaks in an EEG segment in the same way it is done by a human expert who is visually inspecting the signal. It is therefore implemented as a regular zero-crossing calculation of the first derivative, but before this calculation, the signal is transformed in order to keep only the morphological features that are prominent to the human eye. A family of methods well suited for this type of transformation is a polygonal approximation, also called piece-wise linear representation or linear path simplification [23]. These methods assume that the input signal can be represented as a sequence of linear segments, and they apply different techniques to obtain the minimum number of segments that best represent the underlying morphology. Formally:

Definition 2.1 (Polygonal Approximation)**.** Given a time series represented as a sequence of n time-value

points $S = \{(t_0, S_0), \ldots, (t_{n-1}, S_{n-1})\}$, a *polygonal approximation* of S is a subsequence $L \subseteq S$ for which the time series behaviour between any pair of consecutive points $((t_i, S_i), (t_{i+1}, S_{i+1})) \in L$ is assumed to be linear.

Under this general definition, we can determine a broad set of non-linear transformations that potentially remove much information from the original signal, depending on how aggressive the approximation is. A coarse approximation will only retain the most outstanding behaviour of the signal, while a fine-grained approximation will remove only the parts that are not even recognizable by the human eye. This level of detail is fully customizable as a parameter of the approximation transformation.

To illustrate this idea, Figure 1 shows an example of a 20-second EEG segment that is approximated using two different thresholds, according to the algorithm described in Section 2.2. Also, we can see how the AZC calculation varies in two different intervals of each signal. In this segment, a seizure starts in the second 10, and this is clearly seen in the morphology changes of the signal, with higher amplitude and a more regular frequency. Let us put focus on how the result of the approximation changes before and after the seizure onset. While the approximated signal after this point is almost identical in the three cases (and, therefore, the AZC value is basically the same), the morphology is much more variable before the seizure onset. Indeed, in low-amplitude regions (such as between seconds 7 and 8) AZC varies from a very high value in the original signal, to zero in the case of a relatively high approximation threshold. In the middle figure, we can see that visually the signal is very similar to the original one, but the AZC count in the highlighted segment is less than half. What we want to highlight here is that, while the AZC is fundamentally a feature estimating frequency, its calculation is primarily determined by the amplitude behaviour of the signal. Therefore, it simultaneously captures these two dimensions, which are the ones assessed by the experts during visual inspection.

2.2. Approximation Algorithm

There are multiple algorithms to perform the type of morphological approximation we are targeting [23], each of them with different properties, constraints, and computational complexity. Some of them can potentially be implemented in hardware [24] and attached directly to the ADC of the signal sampler, making it possible to directly acquire an approximated signal and, thus, reduce the amount of information to be processed.

Still, the algorithm we selected to perform EEG approximation is the Douglas-Peucker method [25], which requires access to the whole data to guarantee optimality. The main reason for this choice is that

the approximation threshold ϵ is directly a measure of amplitude tolerance. Thus, it is fully interpretable, easy to characterize, and lies on the same scale as the EEG signal. Therefore, to ensure that we provide an acceptable approximation for every subject and channel, we propose to simultaneously calculate the AZC feature using different approximation thresholds to cover, in a logarithmic scale, the full range of physiologically meaningful EEG signals.

The operation of the Douglas-Peucker method is detailed in Algorithm 1. The input is a signal fragment S as a sequence of n samples $(S_0, \ldots, S_{n-1})$, and a threshold $\epsilon > 0$ representing the minimum amplitude difference that can be considered to include a point in the approximation. As output, the algorithm returns a sequence $L = (p_0, \ldots, p_{m-1})$, with $2 \leq m \leq n$, representing the samples selected for the approximation. As we can see, the approximation is initialized by the endpoints 0 and $n-1$ (line 3). At each iteration of the outer loop (lines 5 to 16), the approximation is extended with the point of maximum distance to the segment defined by the linear interpolation (INTERP function) between any consecutive pair of points already included in the approximation (lines 5 and 11). The procedure finishes when none of the points exceeds the minimum amplitude difference (line 6).

Algorithm 1 Douglas-Peucker approximation algorithm

1: **function** DOUGLAS-PEUCKER(S, ϵ)
2:     **let** $n = |S|$
3:     **let** $P = \{(0, S_0), (n-1, S_{n-1})\}$
4:     **let** $S' = \text{INTERP}(S_0, S_{n-1}, n)$
5:     **let** $M, k = max(|S_i - S'_i|), i \in [0, n-1]$
6:     **while** $M > \epsilon$ **do**
7:         $P = P \cup \{(k, S_k)\}$
8:         $M = 0$
9:         **for all** $j \in [0, \ldots, |P| - 2]$ **do**
10:           $S' = \text{INTERP}(S_{k_j}, S_{k_{j+1}}, k_{j+1} - k_j)$
11:           $M', k' = max(|S_i - S'_{i-k_j}|), i \in [k_j, k_{j+1}]$
12:           **if** $M' > M$ **then**
13:              $M, k = M', k'$
14:           **end if**
15:         **end for**
16:     **end while**
17:     **return** $L = \{(t_p, S_p), \ p \in sorted(P)\}$
18: **end function**

---

3. Methodology

This section describes the strategy we adopt to validate the proposed AZC feature. In particular, we assess its discriminative power and potential use for long-term epileptic patient monitoring.

3.1. Feature Discriminative Power

The Kullback-Leibler (KL) divergence is a score widely used in information theory to assess the statistical distance between two probability distributions [22]. The higher the discriminative power, the easier it is to correctly label the data points.

We assess the discriminative power of all features on the epileptic seizure detection (i.e., *ictal* vs. *non-ictal*), comparing the KL divergence of the AZC features against features typically used in the literature. We obtain the KL divergence using (1), where $P(x)$ and $Q(x)$ are the feature probability distributions estimated for *non-ictal* and *ictal* time periods, respectively. Distributions are obtained via a relative frequency histogram drawn from a feature subset $\{X = x_1, x_2, ..., x_n\}$, where histogram bins $\{I_i : i = 1, ..., M\}$ are intervals between X minimum and maximum values. For instance, $P(x)$ is given by the quotient between the number of elements of each bin and X's length.

$$KL(P||Q) = \sum P(x) \cdot \log_2 \frac{P(x)}{Q(x)} \tag{1}$$

3.2. Adopted Machine-Learning Methodology

Automated seizure monitoring still poses considerable challenges for achieving acceptable performance in real-life conditions [9]. First, removable and unobtrusive wearable devices are preferred by PWE [6, 8], which are known by hardware limitations on memory and processing capacity. Thus, low-complexity algorithms for seizure detection are preferable to adhere to the restrictions imposed by such resource-constrained devices. Nevertheless, ML models should still achieve desirable performance metrics to attract usage interest [9]. Such models are trained on long-term time series, and have to be able to deal with high data imbalance. Moreover, regarding EEG/iEEG-based monitoring, seizure patterns vary greatly between subjects, and even for the same subject over time [26]. Also, high amplitude artifacts and cyclic oscillations can confound model training/detection [12].

Targeting a feasible solution for outpatient monitoring, we adopt the RF classification algorithm to assess the AZC performance in the seizure detection task. RF is an algorithm based on an ensemble of decision trees to reduce model overfitting. It is fast and lightweight, both in model size and memory footprint [27], and it has been extensively used for EEG-based seizure classification [20, 16, 28].

Regarding model-training data-related hurdles, it is essential to adopt an assessment methodology that represents real-life usage to avoid achieving unrealistic performance metrics. Thus, we shall avoid employing only a subset of a dataset to assess the performance of the proposed ML algorithms. Even if models are trained using a small subset of the dataset, the evaluation should be done on the available data in general. For example, the performance of some works as [29, 28, 16] tends to be overestimated and impractical when considering the entire data set, as only a small number of data points are used to assess the proposed techniques. This happens as the probability of drawing samples of data presenting artifacts and other common acquisition problems randomly is very low. Second, the data imbalance is a critical point when choosing the appropriate performance metrics. Consequently, in this work, we adopt metrics recommended by the clinical community: sensitivity, FAR [30], and F1 score. Moreover, we consolidate those metrics by seizure episode instead of by the total of data windows used during the inference. Third, patient-specific detectors can overcome the variability of seizure patterns among subjects. Following previous work, we adopt a personalized ML modeling approach [12, 16].

Last, we advocate for a cross-validation (CV) method that takes into account the chronological relation between data points, preserving the temporal dependency among them, and thus representing the assessment of a real-life application more appropriately. For instance, in the leave-one-out CV (LOOCV) method used in [3, 17, 12], withheld data is evaluated with a model trained on all the remaining data. By adopting a non-realistic approach in which future data is used to evaluate the current test set, LOOCV tends to overestimate results. To overcome this problem, we adopt the TSCV approach [31], which is illustrated in Figure 2. In the TSCV scheme, we guarantee that a minimum amount of data is used to train the very first model, which must include at least one seizure. The remaining data is used for testing and divided into several subsets of a minimum of one-hour long files, thus minimizing potential correlation with neighbouring training data. Each of these subsets is tested once, and at each iteration, the latest tested data is added to the training subset. The final performance is then obtained by concatenating the results of each test subset.

3.3. AZC Features

By using different approximation thresholds in the algorithm described in Section 2.2, we can obtain a highly discriminative features that carry both time and frequency characteristics, and account for intra-/inter-patient variability in seizure patterns (i.e., waveform, amplitude, and frequency) [26]. In this work, we obtain six AZC features. The first feature is calculated without the use of the polynomial approximation, thus representing a classical zero-crossing. The other five AZC features are obtained by applying the Douglas Peucker algorithm using 16, 32, 64, 128, and 256 μV as approximation thresholds, hence covering the normal
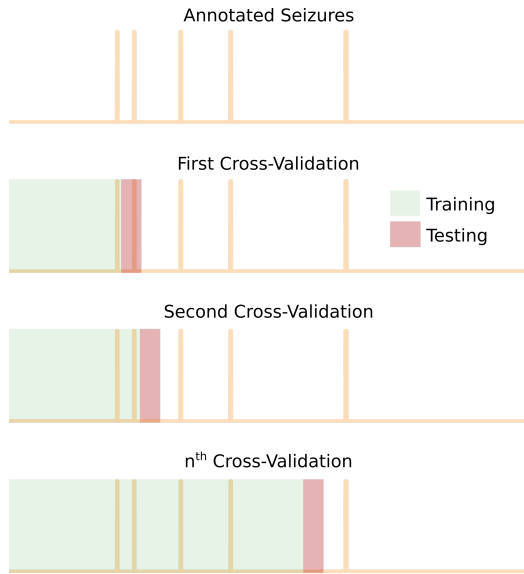
Figure 2. Proposed time-series cross-validation approach.

EEG amplitude range.

3.4. Classical Literature Features

We compare the proposed AZC features against a set of features commonly used for EEG-based seizure detection, hereafter denominated classical literature features (CLF). The used CLF is composed of the 54 features proposed in [16] and two time-domain features (i.e., *line length* and *mean amplitude*), thus yielding the 56 features set described below.

3.4.1. Time Domain Features: we employ the *line length* and the *mean amplitude*, calculating them according to (2) and (3), respectively [32].

$$LL = \frac{1}{N} \sum_{i=1}^{N} (|s_i - s_{i-1}|) \qquad (2)$$

$$MA = \frac{1}{N} \sum_{i=1}^{N} |s_i| \qquad (3)$$

where $\{S = s_1, s_2, ..., s_n\}$ is a time-series of length N.

3.4.2. Frequency Domain Features: ictal activity is known to affect EEG brainwaves [2], thus we rely on the signal spectral power to obtain the EEG bandpower in various frequency bands, namely: delta [0.5, 4] *Hz*, theta [4, 8] *Hz*, alpha [8, 12] *Hz*, beta [13, 30] *Hz*, and gamma [30, 45] *Hz*. Additionally, we include the total power and the power for [0, 0.1] *Hz*, [0.1, 0.5] *Hz*, and [12, 13] *Hz* bands. Furthermore, we also calculate the relative power of the aforementioned bands to the total power, yielding a subtotal of 17 features.

3.4.3. Non-linear Features: we use Shannon (SEn), Tsallis (TEn), Rényi (REn), Sample, and Permutation entropies. These entropies are calculated according to [33, 16], considering a histogram with ten bins and adopting $\alpha = 2$ and $\beta = 2$ to calculate Rényi and Tsallis entropies, following [33]. Before calculating all the entropies, we pre-process the data using discrete wavelet transform employing the Daubechies 4 (DB4) basis function. We obtain the approximated and detailed coefficients down to level seven. As in [16], we obtain a total of 37 features from the detailed coefficients: Sample entropy is calculated from coefficients at levels six and seven; the remaining entropies are calculated from coefficients at levels three, four, five, six, and seven for different input parameters.

3.5. AZC at the Edge

One of the main aims of the AZC feature is to increase seizure detection robustness leveraging classical machine learning (ML) algorithms on edge devices. The computational complexity of AZC is estimated using the e-Glass wearable device based on an ARM Cortex-M4 microcontroller [16, 27].

We adapted our proposed AZC extraction methodology described in Section 2.2 by using the fast algorithm for polygonal approximation proposed in [34] to leverage AZC's real-time implementation in the e-Glass platform. Moreover, we adopt the CMSIS (Cortex Microcontroller Software Interface Standard) to speed-up data processing as it is tailored for fast execution in ARM devices, associated with the CMSIS Real-Time Operating System (CMSIS-RTOS) to enclose our application. Furthermore, we also achieve an optimized CLF extraction by using the CMSIS library and a version of the GNU Scientific Library (GSL) [35] cross-compiled for ARM microcontrollers.

4. Experimental Setup

In this section, we introduce the datasets used in the experiments. Moreover, we detail our experimental setup, for both KL divergence calculation and seizure detection. Finally, we talk about the adopted post-processing approach and the performance metrics used to report our results.

4.1. Datasets

We employ two datasets to evaluate the performance of the proposed features for seizure detection: the CHB-MIT Scalp [12] and the SWEC-ETHZ iEEG datasets [15]. Both are annotated by neurologists and are publicly available[1][2].

[1]https://physionet.org/content/chbmit/1.0.0/
[2]http://ieeg-swez.ethz.ch/

The CHB-MIT includes scalp EEG from 24 children (5 males and 18 females, 10 ± 5.7 years old, one repeated patient), containing a total of 198 annotated seizures. Data are recorded using the bipolar montage (10-20 system [36]) at a sampling frequency of 256 Hz and using 16-bit resolution. A total of 982.9 h of data is available, with only 3.2 *hours* of labelled ictal data (seizure average length of 58.6 ± 65.0 s). The dataset is generally organized in one-hour-long files, in the European data format (*.edf*). However, some subjects have files of two or four hours long, and some files containing ictal data are less than one hour long.

Furthermore, subject *chb12* presents three files with data acquired on a monopolar montage, including 13 seizures. Thus, we excluded these three files to keep a similar methodology among all subjects. As a result, the used CHB-MIT's data has a total of 185 annotated seizures.

The SWEC-ETHZ dataset presents 2656 hours of long-term iEEG data from 18 patients, containing a total of 116 annotated seizures. Data are recorded in a monopolar montage at sampling rates of 512 or 1024 Hz, median-referenced, and band-pass filtered between 0.5 and 120 Hz (zero-phase, 4th-order Butterworth filter). The data are organized as 1 *hour* long *.mat* files accompanied by one extra file per subject, including seizure annotations.

4.2. Data Pre-Processing

First, we decimate the SWEC-ETHZ data to have the same sampling frequency as the CHB-MIT dataset (i.e., 256 Hz). Then, the data of each file is filtered between [1, 20] Hz using a zero-phase, 4th order, Butterworth band-pass filter.

Thereafter, the filtered EEG data is divided into windows of 4 s with a 0.5 s step (87.5% overlapping). We extracted a total of 62 features (56 CLF + 6 AZC features) per EEG window, per EEG channel. For the CHB-MIT dataset, we performed these steps for the 18 common EEG channels among all subjects (that is, FP1-F7, F7-T7, T7-P7, P7-O1, FP1-F3, F3-C3, C3-P3, P3-O1, FP2-F4, F4-C4, C4-P4, P4-O2, FP2-F8, F8-T8, T8-P8, P8-O2, FZ-CZ, CZ-PZ). Hence, it yields a total of 108 AZC and 1008 CLF features that are concatenated in matrices in which the lines are equivalent to the number of EEG windows and columns to the total number of features. However, the SWEC-ETHZ metadata do not include information on the iEEG electrode locations. Furthermore, the number of channels among subjects varies greatly from 32 to 128 [15], so we use all available channels for each subject. Finally, we generate labels for the data representing ictal vs. nonictal data. An EEG window is labelled according to its majority class (e.g., a window having 50% or more ictal data is labelled as ictal).

Next, we reorganize the extracted feature files to contain the equivalent of one hour of data, disregarding the number of seizures available. Moreover, we guarantee that the first file contains at least one seizure and a minimum of five hours of data, which has been arbitrarily chosen.

4.3. KL Divergence and Seizure Detection

We calculate the KL divergence employing histograms with 100 bins. Using box plot visualization of the KL discriminative power among features, we can observe the KL values and also its distribution. We obtain the plot by grouping all subjects' scores per feature, disregarding the EEG channel of origin. Moreover, CHB-MIT is considered more challenging for seizure detection given that scalp EEG acquisitions are prone to suffer from various artifacts (e.g., subject movements, blinking, chewing, electrode disconnections). Consequently, we will only present the CHB-MIT dataset box plot of KL scores in Section 5. However, the SWEC-ETHZ iEEG equivalent plot can be found in the supplementary material.

Regarding the seizure detection problem, we propose an RF-based seizure detection method using only AZC features and assess its performance for both datasets using the TSCV approach. Moreover, we compare the obtained results against the same method employing the CLF set. All available seizures are used for model training and performance assessment. Finally, the code used in this work is made publicly available[3].

4.4. Post-Processing and ML Performance Metrics

Aiming at reducing FAR due to short bursts of rhythmic activity or high amplitude artifacts, we post-process the inferred output's probability of a data window being assigned to *ictal* (S) or *non-ictal* (NS) classes. Using the Bayesian approach proposed in [13], we obtain the posterior classification probability for each EEG window as the dot product of the probabilities of W windows. Second, we apply a tolerance for seizure detection of 10 sec before and 30 sec after the ground truth when determining the number of true positives and false positives, merging all the true positives that occurred for the duration of a ground truth event. Next, we define a measure of classification likelihood (CL), for each ith EEG/iEEG window, as the log-odd of *ictal* over the *non-ictal* posterior probabilities (see (4)). A new classification is then assigned by thresholding the CL values. We adopt W=10 and a threshold of 1.5, according to [13].

$$CL[i] = \log_2 \frac{\sum_j^i S[j]^2}{\sum_j^i NS[j]^2} \qquad (4)$$

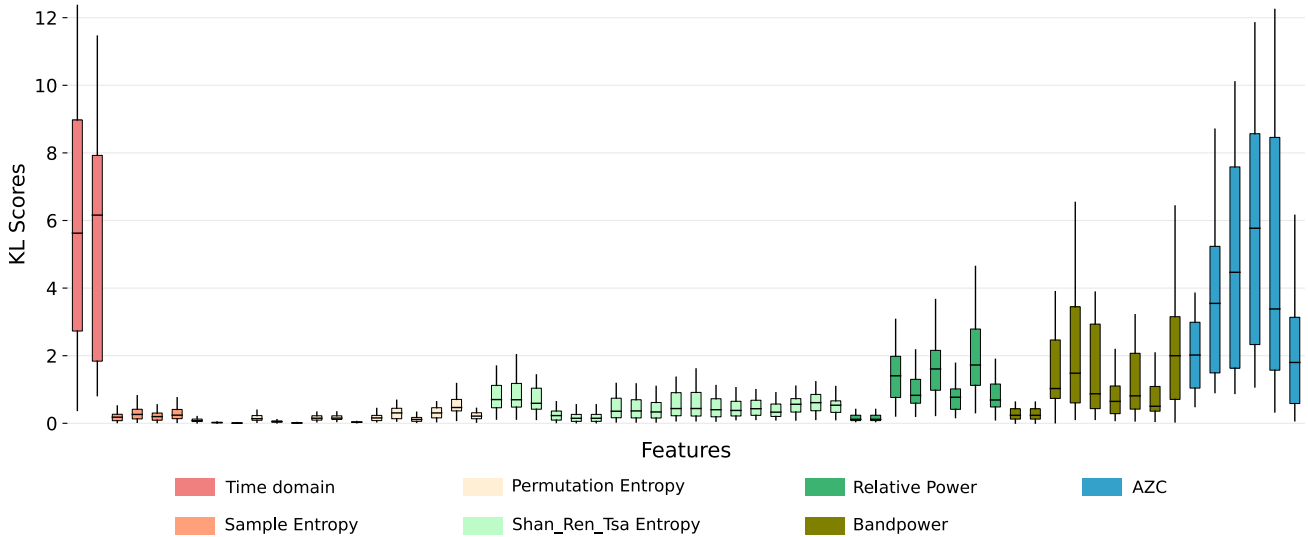[3] https://c4science.ch/source/AZC_Feature_Paper/

Figure 3. KL divergence scores distribution, per feature, for the CHB-MIT dataset. For a detailed description of the features, please refer to Section 3.5.

Table 1. CHB-MIT: number of detected seizures and FAR/day.

Subjects	01	02	03	04	05	06	07	08	09	10	11	12	13	14	15	16	17	18	19	20	21	22	23	24	Tot*
# Seizures	7	3	7	4	5	10	3	5	4	7	3	27	12	8	20	10	3	6	3	8	4	3	7	16	185
# Seiz. Test	5	2	3	3	4	7	2	3	3	6	2	16	11	4	19	9	1	5	2	7	3	2	4	9	132
# Detec. AZC	5	2	2	2	4	4	2	3	3	6	2	16	4	4	16	1	1	2	2	5	2	2	3	9	**102**
# Detec. CLF	5	2	3	2	4	2	1	3	3	6	2	15	3	4	16	0	1	2	2	7	1	2	4	9	99
Data Avail.(h)	41	35	38	156	39	67	67	20	68	50	35	21	33	26	40	19	21	36	30	28	33	31	27	21	979
Data Test (h)	36	20	33	137	33	59	24	15	46	32	2	15	16	21	34	9	16	7	2	18	14	14	21	15	638
FAR/day AZC	0.7	3.6	1.5	0.2	0.7	0.4	0	9.6	0	0	0	11.2	3.0	1.1	3.5	0	0	3.6	0	2.7	0	0	1.1	7.4	**2.1**
FAR/day CLF	3.4	2.4	1.5	0.2	0.7	0.4	0	8.0	0	0	0	11.2	1.5	1.1	2.8	0	1.5	0	0	4.1	0	0	2.3	5.9	2.0

*All the values are a sum for all subjects but the FAR, which are averages.

Table 2. SWEC-iEEG: number of detected seizures and FAR/day.

Subjects	01	02	03	04	05	06	07	08	09	10	11	12	13	14	15	16	17	18	Tot*
# Seizures	2	2	4	14	4	8	4	70	27	17	2	9	7	60	2	5	2	5	244
# Seiz. Test	1	1	3	13	3	7	3	62	24	16	1	8	6	59	1	4	1	4	217
# Detec. AZC	1	1	3	10	3	6	2	47	24	15	1	8	6	58	1	4	1	3	**194**
# Detec. CLF	1	1	3	11	2	6	2	42	12	15	1	8	6	42	1	4	1	3	161
Data Avail.(h)	293	235	158	41	109	146	69	144	41	42	212	191	104	161	196	177	129	205	2652
Data Test (h)	172	5	74	36	103	127	49	126	36	37	29	109	96	73	154	66	46	112	1450
FAR/day AZC	0	0	0	0	1.4	0	0.5	3.6	0	0.6	0	0	0.3	6.5	0	0	2.1	2.1	**1.0**
FAR/day CLF	0	0	0	0	1.2	0	0.5	2.5	0	0	0	0.2	0	1.6	0	0	2.6	1.1	0.5

*All the values are a sum for all subjects but the FAR, which are averages.

where $j = i - W + 1$.

In sequence, we compare the post-processed output against the ground truth to account for: *true positives (Tp), false positives (Fp)*, and *false negatives (Fn)*. These metrics are only given per seizure episode. Additionally, as labels are not always well synced with ictal activity, we add a tolerance before and after a hit (i.e., 10 and 30 s) when checking for *Fp*.

By using the above metrics, we report sensitivity (Sens) and FAR. Moreover, we also compute precision (Prec) and F1 score, thus allowing comparison with other SoA works. These metrics are defined as:

$$Sens = \frac{Tp}{Tp + Fn}, \qquad Prec = \frac{Tp}{Tp + Fp} \qquad (5)$$

$$F1 = \frac{2 \cdot Sens \cdot Prec}{Sens + Prec}, \qquad FAR = \frac{Fp}{total\_time} \qquad (6)$$

where *total_time* corresponds to the total amount of hours of data in the test set.

We assess our real-time implementation of AZC and CLF feature extraction algorithms in terms of runtime and memory requirements to process one EEG data window of 1024 samples. Regarding the timing of the application, we employ the data watchpoint trigger component available on ARM microcontrollers to allow us to count the cycles of the main clock elapsed while processing each block of features. We configure the main clock to its maximum value (i.e., 80 MHz). Furthermore, the memory demands for each strategy are obtained by combining the use of the CMSIS RTOS function *uxTaskGetStackHighWaterMark* for stack usage with a manual account of the allocated dynamic memory.

5. Results

We assess the AZC discriminative power by employing the KL divergence on the probability distributions of *ictal* and *non-ictal* EEG data. Figure 3 displays the distribution of the KL scores for the CHB-MIT dataset. The AZC features extracted for different approximation thresholds exhibit KL scores higher than most of the other features. For instance, three out of the five highest median scores are from AZC features obtained with different approximation thresholds (e.g., AZC for 64 μV presents the second-highest median score). Only the *line length* and *mean amplitude* present comparable scores among the 56 CLF features. Meanwhile, features commonly used in SoA works as power features (mainly delta, theta, and alpha bandpower) present relatively smaller scores, followed by Renyi, Tsallis, and Shannon entropies. The remaining features achieved very small discriminative power. In any case, those features with lesser scores are still useful as they can improve separability when combined with others.

Regarding the seizure detection assessment, as specified in Section 3.2, we report results for a patient-specific detection approach. Table 1 and Table 2 present the main detection results (i.e., sensitivity and FAR). Overall, we observe that the AZC-based method detected a higher number of seizures compared to the CLF-based one: 102 and 194 against 99 and 161, for CHB-MIT and SWEC-ETHZ, respectively. While, it keeps a similar FAR/day of an average of 2.1 and 1.0 against 2.0 and 0.5, per day, respectively. Moreover, Figure 4 shows the F1 score, sensitivity, and precision, per subject, for both datasets and approaches tested (i.e., AZC- versus CLF-based detection). AZC-based detection outperforms the CLF-based one in average performance values for most of the subjects. Overall, 71.4% of patients reached an F1 score greater than 70%, with 84.8% of the tested seizures detected.

Finally, the embedded microcontroller implementation of the AZC feature calculates the six target features in only 2.98 ms, against the 26.45 ms taken by the algorithm to calculate 56 features. Finally, in terms of RAM memory, the AZC algorithm demands up to 4160 bytes while the CLF calculation takes 4774 bytes.

6. Discussion

The evaluated AZC features achieve higher median KL scores than most of the other features (see Figure 3) but also present a wide range of values. Those values are obtained using all available EEG channels among all patients. Thus, the lack of epileptiform activity in some scalp regions may reduce the separability among data. Moreover, ictal patterns vary greatly among patients, and some patterns can be identified easier than others [26]. Therefore, AZC could potentially achieve higher discriminative power in case we employ a channel selection approach per patient. Another limitation of our work is related to the set of thresholds used to calculate the AZC values. Regarding seizure patterns difference among patients, a personalized selection of thresholds might also boost AZC's discriminativeness.

Nevertheless, the employed method for extracting AZC features reaches very high performance in both datasets (i.e., 25 subjects out of 42 achieve 100% sensitivity, plus nine showing only one missing seizure). Additionally, we also achieve a very low FAR/day: 2.1 and 1.0/day on average for CHB-MIT and SWEC-iEEG, respectively. These results are achieved using only six features per channel, as opposed to the 56 used in the CLF-based method. Considering the simplicity of the algorithm to calculate the proposed feature (i.e., AZC's calculation is 8.8x faster than the CLF ones and demands less RAM memory), these results support our final goal of using AZC in resource-constrained wearable devices for long-term monitoring of PWE. Although of low complexity, the AZC feature presents an intrinsic ability to capture changes both in time and in the frequency domain. For example, by approximating the EEG signal under different thresholds, we capture changes in the amplitude of the EEG during an ictal event [37]. Furthermore, the synchronicity of ictal-EEG (that is, slow wave discharges at 3–5 Hz [37]) is also captured by the proposed zero crossing count, while the different thresholds increase the separability of the ictal/non-ictal data.

More importantly, these results were obtained using a particularly demanding TSCV methodology for assessing the classification performance, where models are trained on an incremental amount of data. To the best of our knowledge, the proposed TSCV approach has not yet been used for assessing seizure detection methods based on EEG/iEEG. Due to its interactive training manner, the TSCV approach makes the assessment harder than other methods
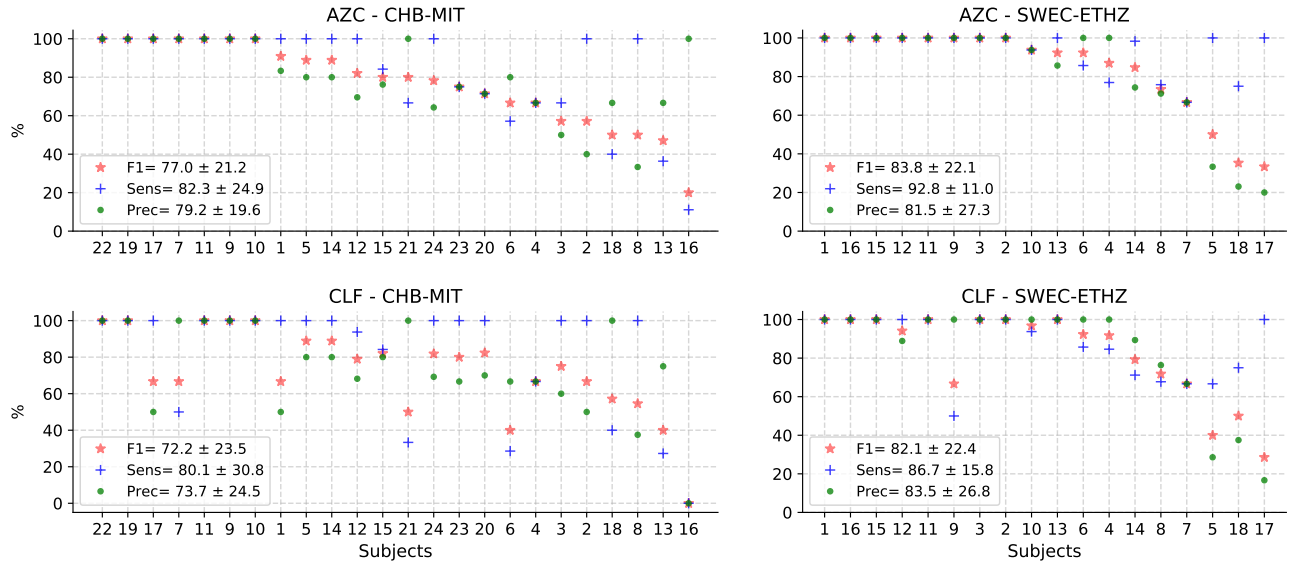
Figure 4. Performance metrics obtained with AZC-/CLF-based classification approaches, on both datasets.

commonly found in the literature, and it is not directly comparable in terms of accuracy. Depending on the available amount of seizures per subject and their position in the acquisition timeline, most TSCV trained models face an even higher data imbalance rate when compared to LOOCV models. The lack of ictal data can cause more misclassifications and false alarms, as can be observed for some subjects' timelines in the supplementary material (e.g., *chb03*, *chb07*, *id07*). However, TSCV maintains chronological data relations, thus providing a more realistic assessment for long-term seizure monitoring approaches.

The LOOCV approach may provide the closest comparison when used to evaluate performance using the whole dataset. For instance, [12] indicates high sensitivity in the CHB-MIT dataset even for subjects declared difficult. By using all seizures but one for training, and by declaring a seizure detection based on only one positive prediction, [12]'s method achieves high sensitivity at the cost of a higher FAR. Although not employing any post-processing, [12] indicates a low average FAR of 3.12/day, which might be explained by the fact that it was only assessed on files without seizures. We report FAR for all tested data, including post-ictal data and in-between sequences of seizures. For instance, by avoiding files containing ictal data, FAR values for *chb12* are not realistic and not comparable to the ones reported in this work (*chb12* has only 11 files with zero seizures out of the 29 currently available). Moreover, this work also reports a relatively high FAR for subject *chb24*, which has not been included in [12].

A similar approach to classification performance evaluation is used by [17] in its patient-specific and hybrid models. The use of fully-connected convolutional neural networks (CNN) trained in most

of the data available, but one record, produced models with high sensitivity to ictal data, but using rather complex architecture dependant on the tuning of 1000 hyperparameters. Besides the inherent over-optimistic results associated to the LOOCV methodology, as discussed above, by considering only one positive classified window, the minimum need for asserting a seizure detection, [17]'s sensitivity is reported as 100%. Additionally, it also reports low average FAR but, once more, calculated only on records not presenting seizures. Thus, [17] did not assess FAR for all available data and, more specific, it did not employ records with a higher probability of presenting false-alarms due to the proximity to true events (as can be seen in the classification timelines of *chb08*, *chb12*, and *chb15*, in the supplementary material).

Other works, such as [14], employ a generalized model in their classification approach and are also not directly comparable with our personalized approach. Also using CNN, [14] reports fair metrics for CHB-MIT in a per-window assessment approach (F1 score of 0.59 ± 0.26) when employing 80% of each subject's first seizures to train its best model. Thus, this work's results corroborate the requirement of a higher amount of ictal data to improve classification performance.

Regarding the SWEC-ETHZ iEEG dataset, the sensitivity we obtained is similar to [15]'s (194 seizures detected out of 217 versus 72 out of 92). However, two remarks are relevant regarding the methodological differences. First, [15] employs the concept of leading seizures for subjects *id08* and *id14*, thus reporting results only for the very first seizure in the long sequence of ictal activity observed in the data of subjects *id08* and *id14* (Figure 5 and Figure 6).This affects sensitivity, as well as, FAR results for both subjects. Considering

that those ictal periods are rather long (up to 10 hours for *id14*), we decided to report results for all events. Moreover, [15]'s FAR (average 1.44/day) is considered overestimated as its post-processing is tailored per subject, a rather data-dependent approach.

In relation to specific patient results, we would like to draw attention to some patients that are regarded as difficult cases. For instance, patients *chb6* and *chb16* are well known for their short seizures, i.e., 15.3 ± 2.9 s, and 8.4 ± 2.3 s, respectively. Thus, they present less ictal data for model training. Nonetheless, the AZC-based detection still performs relatively well for *chb6*. Such performance might be explained by *chb06*'s EEG morphological pattern, which shows a decreasing signal amplitude and increasing frequency during seizures. In such a case, the approximation algorithm associated with the AZC feature calculation approach would further affect the zero-crossing counts, as illustrated in Figure 1, thus increasing its discriminative power. Another CHB-MIT particularity, pointed out in [12], is that patient *chb13*'s non-ictal data contains short bursts of rhythmic activity similar to its typical seizure patterns. Hence, it introduces a confounding effect to the proposed algorithm, which uses all available data for training. At last, [26] reported the existence of three unlabeled seizures in *chb24*'s data, immediately after its second-last seizure, which could correspond to the false positives shown in Figure 7 around the 11*th* hour.

Regarding the SWEC iEEG dataset, subjects *id08* and *id14* present a long-lasting cluster of ictal activity labelled as various single events in sequence. As can be seen in Figure 5 and in Figure 6, most of the missed detection and false positives accounted for in both subjects are closer to the cluster boundaries. In a real-life application, such cases would be rather acceptable as detections are close to true ictal events.

Finally, the use of a wide variety of features can boost seizure detection in some cases. For example, the CLF-based methodology detected more seizures than the AZC-based one for some subjects (i.e., *chb03*, *chb20*, *id04*), presenting lower FAR for seven subjects from both datasets, as can be seen in Tables 1 and 2. These results might be explained by the intrapatient variability in seizure patterns and the presence of various artifacts along the recordings, which requires a fine-grained trained decision boundary to achieve higher performance. However, the AZC-based approach presents results on par for most of the subjects assessed.

7. Conclusion

In this work, we have introduced a new interpretable and highly discriminative feature for long-term monitoring of epilepsy, namely approximate zero-crossing (AZC). Inspired by neurologists' procedures in interpreting
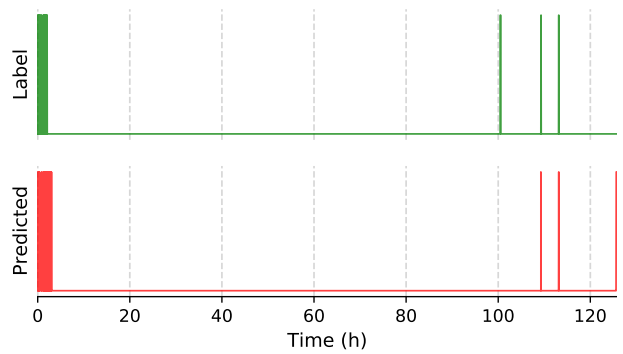

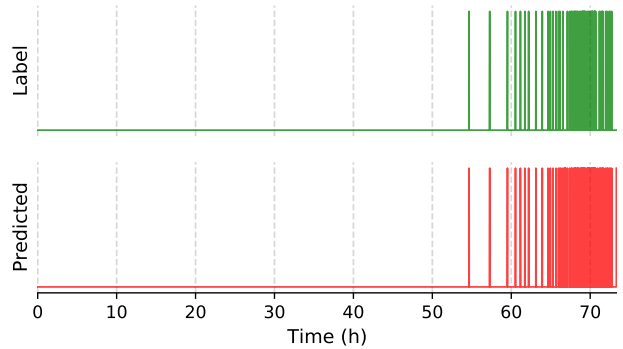**Figure 5.** AZC prediction for SWEC subject *id08*.

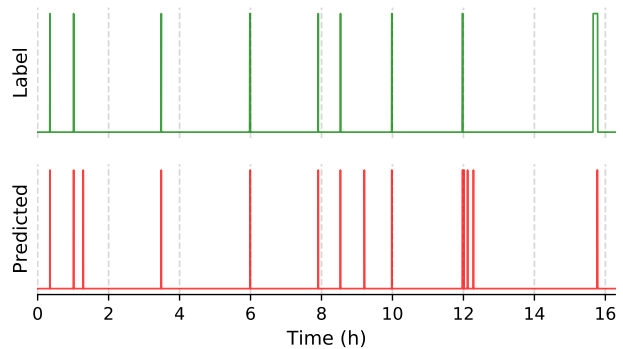**Figure 6.** AZC prediction for SWEC subject *id14*.

Figure 7. AZC prediction for CHB-MIT subject *chb24*.

and labelling EEG and iEEG data in clinical practice, the AZC feature also targets to mimic how our brain selectively picks prominent patterns among noisy data. We have employed the KL divergence to show AZC's high discriminative power over a classical set of features used in the SoA. Moreover, we have assessed AZC performance in seizure classification using two publicly available long-term datasets (i.e., CHB-MIT - 982.9 hours, and SWEC-ETHZ - 2656 hours). Overall, an AZC-based classification method detected 102 and 194 seizures against 99 and 161, for the CLF-based one (CHB-MIT and SWEC-ETHZ datasets, respectively), with significantly less features (6 for AZC and 56 for CLF). While, it kept a similar FAR/day, i.e., average of 2.1 and 1.0 against 2.0 and 0.5, per day. Thus, the

proposed AZC feature may contribute to developing new methods for outpatient monitoring, particularly on wearable devices, due to its low complexity and high discriminative power.

8. Acknowledgements

References

[1] World Health Organization. *Neurological disorders : public health challenges*. 2006. URL: https://apps.who.int/iris/handle/10665/43605 (visited on 06/06/2022).

[2] W.O. Tatum et al. "Clinical utility of EEG in diagnosing and monitoring epilepsy in adults". In: *Clin Neurophysiol.* 129.5 (2018), pp. 1056–1082. DOI: 10.1016/j.clinph.2018.01.019.

[3] Lasitha S Vidyaratne and Khan M Iftekharuddin. "Real-Time Epileptic Seizure Detection Using EEG". In: *IEEE Trans. Neural Syst. Rehabil. Eng.* 25.11 (2017), pp. 2146–2156. DOI: 10.1109/TNSRE.2017.2697920.

[4] Howard J Faulkner, Hisatomi Arima, and Armin Mohamed. "The utility of prolonged outpatient ambulatory EEG". In: *Seizure* 21.7 (2012), pp. 491–495. DOI: 10.1016/j.seizure.2012.04.015.

[5] Janice L. Smolowitz et al. "Diagnostic Utility of an Epilepsy Monitoring Unit". In: *Am J Med Qual* 22.2 (2007), pp. 117–122. DOI: 10.1177/1062860606298295.

[6] Christian Hoppe et al. "Novel techniques for automated seizure registration: Patients' wants and needs". In: *Epilepsy Behav.* 52 (2015), pp. 1–7. DOI: 10.1016/j.yebeh.2015.08.006.

[7] Jay Pathmanathan et al. "Expert Perspective: Who May Benefit Most From the New Ultra Long-Term Subcutaneous EEG Monitoring?" In: *Front. Neurol.* 12 (2022). DOI: 10.3389/fneur.2021.817733.

[8] Elisa Bruno et al. "Wearable technology in epilepsy: The views of patients, caregivers, and healthcare professionals." In: *Epilepsy Behav.* 85 (2018), pp. 141–149.

[9] Ilona Hubbard, Sandor Beniczky, and Philippe Ryvlin. "The Challenging Path to Developing a Mobile Health Device for Epilepsy: The Current Landscape and Where We Go From Here." In: *Front. Neurol.* 12 (2021), p. 740743. DOI: 10.3389/fneur.2021.740743.

[10] Sándor Beniczky et al. "Automated seizure detection using wearable devices: A clinical practice guideline of the International League Against Epilepsy and the International Federation of Clinical Neurophysiology". In: *Clin Neurophysiol.* 132.5 (2021), pp. 1173–1184. DOI: 10.1016/j.clinph.2020.12.009.

[11] Yao Guo et al. "Epileptic Seizure Detection by Cascading Isolation Forest-Based Anomaly Screening and EasyEnsemble". In: *IEEE Transactions on Neural Systems and Rehabilitation Engineering* 30 (2022), pp. 915–924. DOI: 10.1109/TNSRE.2022.3163503.

[12] Ali Hossam Shoeb. "Application of Machine Learning to Epileptic Seizure Onset Detection and Treatment". PhD thesis. Massachusetts Institute of Technology, 2009, p. 162. DOI: 10.13026/C2K01R.

[13] Valentin Gabeff et al. "Interpreting deep learning models for epileptic seizure detection on EEG signals". In: *Artif Intell Med* 117 (2021), p. 102084. DOI: 10.1016/j.artmed.2021.102084.

[14] Catalina Gómez et al. "Automatic seizure detection based on imaged-EEG signals through fully convolutional networks". In: *Sci. Rep.* 10.1 (2020), pp. 1–13. DOI: 10.1038/s41598-020-78784-3.

[15] Alessio Burrello et al. "Laelaps: An Energy-Efficient Seizure Detection Algorithm from Long-term Human iEEG Recordings without False Alarms". In: *DATE 2019.* IEEE, 2019, pp. 752–757. DOI: 10.23919/DATE.2019.8715186.

[16] Dionisije Sopic, Amir Aminifar, and David Atienza. "e-Glass: A Wearable System for Real-Time Detection of Epileptic Seizures". In: *2018 IEEE Inter. Symp. on Cir. and Sys. (ISCAS).* Florence, Italy: IEEE, 2018, pp. 1–5. DOI: 10.1109/ISCAS.2018.8351728.

[17] Adam Page, Colin Shea, and Tinoosh Mohsenin. "Wearable seizure detection using convolutional neural networks with transfer learning". In: *2016 IEEE Inter. Symp. on Circuits and Systems.* IEEE, 2016, pp. 1086–1089. DOI: 10.1109/ISCAS.2016.7527433.

[18] Yusuf Uzzaman Khan, Nidal Rafiuddin, and Omar Farooq. "Automated seizure detection in scalp EEG using multiple wavelet scales". In: *2012 IEEE International Conference on Signal Processing, Computing and Control.* 2012, pp. 1–5. DOI: 10.1109/ISPCC.2012.6224361.

[19] Yun Park et al. "Seizure prediction with spectral power of EEG using cost-sensitive support vector machines". In: *Epilepsia* 52.10 (2011), pp. 1761–1770. DOI: 10.1111/j.1528-1167.2011.03138.x.

[20] Mohammad Khubeb Siddiqui et al. "A review of epileptic seizure detection using machine learning classifiers". In: *Brain Informatics* 7.1 (2020), pp. 1–18. DOI: 10.1186/s40708-020-00105-1.

[21] Abhijit Bhattacharyya and Ram Bilas Pachori. "A Multivariate Approach for Patient-Specific EEG Seizure Detection Using Empirical Wavelet Transform". In: *IEEE Trans. Biomed. Eng.* 64.9 (2017), pp. 2003–2015. DOI: 10.1109/TBME.2017.2650259.

[22] Fernando Perez-Cruz. "Kullback-Leibler divergence estimation of continuous distributions". In: *2008 IEEE Inter. Symp. on Information Theory*. 2008, pp. 1666–1670. DOI: 10.1109/ISIT.2008.4595271.

[23] Eamonn Keogh et al. "Segmenting time series: A survey and novel approach". In: *Data mining in time series databases*. World Scientific, 2004, pp. 1–21.

[24] Silvio Zanoli et al. "An Error-Based Approximation Sensing Circuit for Event-Triggered, Low Power Wearable Sensors". In: *ArXiV preprint* (2021). URL: http://arxiv.org/abs/2106.13545.

[25] DH Douglas and TK Peucker. "Algorithms for the reduction of the number of points required to represent a digitized line or its caricature". In: *Int. J. Geogr. Inf. Syst.* 10.2 (1973), pp. 112–122.

[26] Dionisije Sopic et al. "Personalized seizure signature: An interpretable approach to false alarm reduction for long-term epileptic seizure detection". In: *Epilepsia* n/a.n/a (2022). DOI: 10.1111/epi.17176.

[27] Renato Zanetti et al. "Real-Time EEG-Based Cognitive Workload Monitoring on Wearable Devices". In: *IEEE Trans. Biomed. Eng.* 69.1 (2022), pp. 265–277. DOI: 10.1109/TBME.2021.3092206.

[28] Renato Zanetti, Amir Aminifar, and David Atienza. "Robust Epileptic Seizure Detection on Wearable Systems with Reduced False-Alarm Rate". In: *2020 Conf Proc IEEE Eng Med Biol Soc*. IEEE, 2020, pp. 4248–4251. DOI: 10.1109/EMBC44109.2020.9175339.

[29] Thorir Mar Ingolfsson et al. "Towards Long-term Non-invasive Monitoring for Epilepsy via Wearable EEG Devices". In: *2021 IEEE Bio. Circuits and Systems Conference*. IEEE, 2021, pp. 01–04. DOI: 10.1109/BioCAS49922.2021.9644949.

[30] Sándor Beniczky and Philippe Ryvlin. "Standards for testing and clinical validation of seizure detection devices". In: *Epilepsia* 59.October 2017 (2018), pp. 9–13. DOI: 10.1111/epi.14049.

[31] Abdulrahim Mohammed et al. "Time-Series Cross-Validation Parallel Programming using MPI". In: *2021 Inter. Conf. on Data Analytics for Business and Industry*. IEEE, 2021, pp. 553–556. DOI: 10.1109/ICDABI53623.2021.9655795.

[32] Alessio Burrello et al. "An Ensemble of Hyperdimensional Classifiers: Hardware-Friendly Short-Latency Seizure Detection With Automatic iEEG Electrode Selection". In: *IEEE J. Biomed. Health Inform.* 25.4 (2021), pp. 935–946. DOI: 10.1109/JBHI.2020.3022211.

[33] U Rajendra Acharya et al. "Application of entropies for automated diagnosis of epilepsy using EEG signals: A review". In: *Knowledge-Based Systems* 88 (2015), pp. 85–96. DOI: 10.1016/j.knosys.2015.08.004.

[34] Karin Wall and Per-Erik Danielsson. "A fast sequential method for polygonal approximation of digitized curves". In: *Computer Vision, Graphics, and Image Processing* 28 (2 1984), pp. 220–227. ISSN: 0734189X. DOI: 10.1016/S0734-189X(84)80023-7.

[35] Brian Gough. *GNU scientific library reference manual*. Network Theory Ltd., 2009.

[36] G H Klem et al. "The ten-twenty electrode system of the International Federation. The International Federation of Clinical Neurophysiology." In: *Electroencephalogr. clin. neurophysiol.* 52 (1999), pp. 3–6.

[37] S J M Smith. "EEG in the diagnosis, classification, and management of patients with epilepsy". In: *Journal of Neurology, Neurosurgery & Psychiatry* 76.suppl 2 (2005), pp. ii2–ii7. ISSN: 0022-3050. DOI: 10.1136/jnnp.2005.069245.